Biochemistry

Article

pubs.acs.org/biochemistry

Nucleosome Histone Tail Conformation and Dynamics: Impacts of Lysine Acetylation and a Nearby Minor Groove Benzo[*a*]pyrene-Derived Lesion

Iwen Fu,[†] Yuqin Cai,[†] Nicholas E. Geacintov,[‡] Yingkai Zhang,[‡,§] and Suse Broyde*[,†]

[†]Department of Biology and [‡]Department of Chemistry, New York University, 100 Washington Square East, New York, New York 10003, United States

[§]NYU-ECNU Center for Computational Chemistry at NYU Shanghai, Shanghai 200062, China

Supporting Information

ABSTRACT: Histone tails in nucleosomes play critical roles in regulation of many biological processes, including chromatin compaction, transcription, and DNA repair. Moreover, post-translational modifications, notably lysine acetylation, are crucial to these functions. While the tails have been intensively studied, how the structures and dynamics of tails are impacted by the presence of a nearby bulky DNA lesion is a frontier research area, and how these properties are impacted by tail lysine acetylation remains unexplored. To obtain molecular insight, we have utilized all atom 3 μs molecular dynamics simulations of nucleosome core particles (NCPs) to determine the impact of a nearby DNA lesion, 10*S* (+)-*trans*-*anti*-B[*a*]P-N^2-dG—the major adduct derived from the procarcinogen benzo[*a*]pyrene—on H2B tail behavior in unacetylated and acetylated states. We similarly studied lesion-free NCPs to investigate the normal properties of the H2B tail in both states. In the lesion-free NCPs, charge neutralization upon lysine acetylation causes release of the tail from the DNA. When the lesion is present, it stably engulfs part of the nearby tail, impairing the interactions between DNA and tail. With the tail in an acetylated state, the lesion still interacts with part of it, although unstably. The lesion's partial entrapment of the tail should hinder the tail from interacting with other nucleosomes, and other proteins such as acetylases, deacetylases, and acetyl-lysine binding proteins, and thus disrupt critical tail-governed processes. Hence, the lesion would impede tail functions modulated by acetylation or deacetylation, causing aberrant chromatin structures and impaired biological transactions such as transcription and DNA repair.

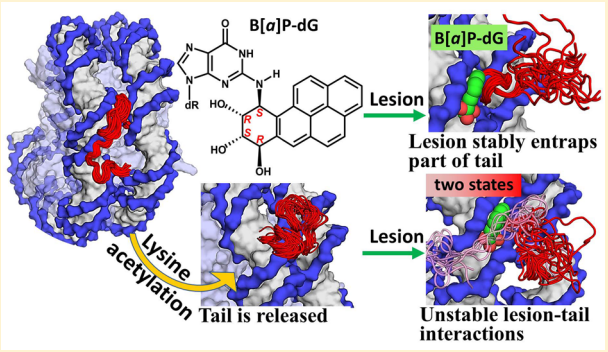

The nucleosome is the basic structural unit of chromatin;[1] the nucleosome core particle (NCP) is composed of 145−147 bp of DNA wrapped left-handed with ∼1.65 superhelical turns around the histone octamer, which contains an $(H3-H4)_2$ tetramer and two (H2A−H2B) dimers, as well as positively charged histone tails that protrude from the histone octamer.[2,3] The histone octamer compacts DNA tightly into superhelical turns, and the histone tails have multiple functions, including mediating folding of nucleosomes into higher-order structures.[4]

The N-terminal histone tails are targets for post-translational modifications (PTMs) that modulate the functions of the histone tails and thereby contribute to the regulation of various vital cellular processes.[5−7] The PTMs on the tails directly mediate the packing of the nucleosomes into higher-order chromatin structures[4] through their contacts with the DNA wrapped around the histone octamer,[8] linker DNA,[9] and the acidic patch regions in neighboring nucleosomes.[10] The PTMs on the tails attract histone modifiers that induce or remove modifications[11] and serve as platforms to recruit chromatin binding proteins for chromatin remodeling.[12−16]

Lysine acetylation of the N-terminal tails is a key, charge-neutralizing, PTM that is involved in the regulation of many biological processes,[17,18] including transcription[19,20] and DNA repair;[7,21−27] it is often deemed to be an epigenetic regulator in the broad sense, as a DNA-related regulatory mechanism that does not involve changes in the nucleotide sequence, regardless of whether it is strictly heritable.[15] Hyperacetylation of histone tails in lightly packed euchromatin is associated with activation of transcription and repair, while hypoacetylation of the tails in tightly packed heterochromatin is associated with their repression. Errors in acetylation or deacetylation may contribute to aberrant chromatin structure and gene expression and thereby perturb cellular processes. Such disturbance may lead to human diseases, including cancer,[28] inflammatory diseases,[29] Huntington's disease,[30] and aging-associated diseases.[31]

Received: November 29, 2016
Revised: March 1, 2017
Published: March 17, 2017

ACS Publications © 2017 American Chemical Society

DOI: 10.1021/acs.biochem.6b01208
Biochemistry 2017, 56, 1963−1973

Each histone tail appears to have unique, essential functions that perform complex roles in regulating chromatin structure.[5,32] The individual tails play crucial and distinct roles in the stability of the nucleosome structure[32−34] and in the compaction of chromatin fibers[35−37] and, consequently, the governance of gene expression.

The H2B tail plays an important role in gene expression and DNA repair.[23,38−41] Studies with yeast have demonstrated that deletion of the H2B N-terminal domain residues 30−37 results in reduced nucleotide excision repair (NER) efficiency and contributes to increased ultraviolet (UV) sensitivity,[38] and that mutants that include deletion of this domain have enhanced nucleosome mobility and better access to nucleosomal DNA.[23] Deletion of the H2B tail in yeast cells upregulates a large number of yeast genes and causes significant loss of histone occupancy, which may cause partially assembled nucleosomes to be unstable; these observations revealed the essential role of this tail in repressing transcription[23,38] and in nucleosome assembly.[39,41] The key role of the H2B tail in regulating transcription is also shown in a study with human HeLa cells, which found that when the H2B tail is in its unacetylated state, Lys20 binds tumor suppressor P14ARF and thereby mediates transcription repression of cell cycle regulatory genes; this repression is lifted by tail acetylation.[40]

Intensive experimental[35−37,42−47] and computational[48−56] studies have revealed a wealth of information about how lysine acetylation on the histone tails affects nucleosome and chromatin structures, yet how the structures and dynamics of tails are impacted by the presence of a nearby bulky DNA lesion is a frontier research area. The influence of such a bulky DNA lesion on unacetylated tail properties has been investigated, to the best of our knowledge, only in our prior study.[57] Moreover, how the interactions between the lesion and the tail are impacted by histone tail lysine acetylation remains unexplored.

Benzo[*a*]pyrene (B[*a*]P) is the most well-studied member of a class of widespread environmental procarcinogens known as polycyclic aromatic hydrocarbons (PAHs) and is classified by the IARC[58] (International Agency for Research on Cancer) as a human carcinogen. B[*a*]P is metabolically activated through the well-studied diol epoxide pathway[59] to the major reactive (+)-*anti*-benzo[*a*]pyrene diol epoxide (B[*a*]PDE), which is highly mutagenic[60,61] and tumorigenic.[62,63] B[*a*]PDE attacks DNA to form the predominant[64,65] and mutagenic[66] 10*S* (+)-*trans*-*anti*-B[*a*]P-N^2-dG (B[*a*]P-dG) bulky adduct to DNA. It adopts a minor groove position in B-DNA in solution.[67] Studies with nucleosomes utilizing B[*a*]PDE to form adducts have found that rotational settings of guanines in the nucleosomal DNA do not explain the observed level of adduction but that the level of adduction was lowest near the dyad.[68]

Here we have carried out a comprehensive investigation of the effect of lysine acetylation on the properties of the H2B tail and its interactions with DNA, and we delineate how the B[*a*]P-dG lesion impacts the tail's behavior in unacetylated and acetylated states. We carried out a series of ∼3 μs molecular dynamics simulations with extensive analyses for four nucleosome core particle (NCP) models: (1) lesion-free NCP with unacetylated tail (*lesion-free/unacetylated* NCP), (2) lesion-free NCP with acetylated tail (*lesion-free/acetylated* NCP), (3) lesion-containing NCP with unacetylated tail (*lesion-containing/unacetylated* NCP), and (4) lesion-containing NCP with acetylated tail (*lesion-containing/acetylated* NCP). The lesion was placed at superhelical location (SHL) ∼ 3 near the investigated full length H2B tail in a NCP. Our results reveal that as anticipated, the charge neutralization upon lysine acetylation causes release of the tail from the lesion-free DNA, while the tail is collapsed on the DNA surface when unacetylated. When the B[*a*]P-dG lesion is present, it stably engulfs part of the nearby histone H2B tail, impairing the interactions between DNA and tail observed in the lesion-free case. Moreover, the lesion still interacts with part of the tail when it is acetylated, although unstably.

Our finding that the tail is released from nucleosomal DNA upon its acetylation supports the understanding that acetylation leads to chromatin opening for access to the DNA,[45−47] and recruitment of other proteins that regulate processes such as transcription and DNA repair.[12−16] On the other hand, the presence of the lesion, regardless of whether the tail is acetylated, causes the tail to be confined by its entrapment that would impair these normal tail functions.

MATERIALS AND METHODS

To elucidate the impact of a minor groove-situated B[*a*]P-dG lesion on the structures and dynamics of a histone tail in unacetylated and acetylated states, we performed MD simulations for the following four NCP models containing the H2B tail at SHL ∼ 3: without further modifications (*lesion-free/unacetylated* NCP), with all lysine residues acetylated on the H2B tail (*lesion-free/acetylated* NCP), with a minor groove-situated B[*a*]P-dG lesion at SHL ∼ 3 (*lesion-containing/unacetylated* NCP), and with lesion and tail acetylation (*lesion-containing/acetylated* NCP). The NCP model with lesion modification site and the histone tail lysine modification sites are shown in Figure 1.

Initial Nucleosome Core Particle Models for MD Simulations. We built an initial model for our simulations that contains only one full length tail, the histone H2B tail (Figure 1A). This initial model is a hybrid NCP model. We began with the NCP with PDB[69] entry 2NZD[70] in which all the histone tails are truncated, including the H2B tail of interest at SHL ∼ 3, whose coordinates for residues 1−27 from the N-terminus were not deposited in the PDB. We modeled in these residues based on the NCP with PDB[69] entry 1KX5[3], in which full length tails were generally resolved; however, many atoms of amino acids in the NCP tails have zero occupancies and/or very high thermal factors. Accordingly, we did not model the first three residues of the H2B tail because the coordinates are missing. The H2B tail at SHL ∼ 3 is between the two DNA gyres (Figure 1B). Note that 1KX5[3] contains the same histones as 2NZD.[70] All other models for our simulations were based on this hybrid model (*lesion-free/unacetylated* NCP). We acetylated all the lysine residues in the H2B tail (see Figure 1C for the tail sequence) for our simulation to investigate the impact of lysine acetylation (*lesion-free/acetylated* NCP); this optimizes the possibility of defining the structural and dynamic impacts of acetylation. Furthermore, we were interested in understanding whether the tail structures and dynamics were impacted by the lesion. Accordingly, we modeled in the minor groove-situated B[*a*]P-dG lesion, based on the NMR solution structure[67] (see the inset box in Figure 1) at SHL ∼ 3, where the H2B tail is nearby and the lesion in the minor groove faces the tail (*lesion-containing/unacetylated* NCP) (Figure S1). We selected the only guanine in this vicinity that situates the B[*a*]P-dG lesion in the minor groove, facing outward toward the H2B tail. The local DNA 11-mer sequence for each gyre and the precise

DOI: 10.1021/acs.biochem.6b01208
Biochemistry 2017, 56, 1963−1973

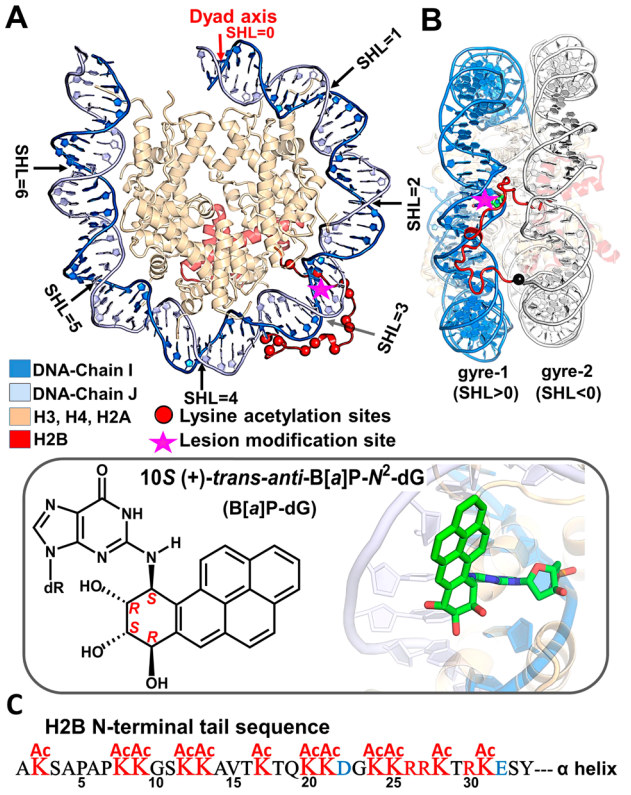

Figure 1. NCP structure and positioning of histone H2B and its tail on the DNA in the investigated model. The model is based on crystal structures of PDB[69] entries 2NZD[70] and 1KX5,[3] as described in Materials and Methods. (A) Best representative structure in the *lesion-free/unacetylated* NCP. Only half of the nucleosomal DNA, with SHL > 0 (corresponding to gyre-1), is shown for the sake of clarity. The location of each base pair with respect to the histone core is designated by its superhelical location relative to the dyad position. The 2-fold pseudosymmetry dyad axis is indicated. The dyad that is at the center of the 145 bp DNA duplex has SHL = 0. The SHL increases by 1 unit for each successive turn of the double helix (~10 bp) in gyre-1, and the positions of the SHLs at 0−6 are indicated. The tail is at SHL ~ 3, and the Cα atom of the first residue from the N-terminus is shown as a black dot. (B) Side view of the NCP structure showing the tail protruding between the two DNA gyres. Gyre-2 corresponds to the DNA double helix location with SHL < 0 (colored gray). The lesion modification site is indicated with a pink star, and the modified strand is chain I from PDB[69] entry 2NZD.[70] The inset box shows the chemical structure (left) of the 10*S* (+)-*trans*-*anti*-B[*a*]P-*N*^{2}-dG (B[*a*]P-dG) lesion and the best representative structure in the *lesion-containing* NCP (right). The B[*a*]P ring system is oriented in the 5′-direction of chain I, and Watson−Crick pairing at the lesion site is maintained in the simulation as in the NMR solution structure.[67] The B[*a*]P-dG lesion is colored by atom with carbons colored green. Lysine acetylation sites on the H2B N-terminal tail are designated as red spheres. (C) Sequence of the H2B N-terminal tail, including the residue numbering (corresponding to the numbers in chain D of the crystal structure of PDB[69] entry 1KX5[3]) and sites for lysine acetylation (Ac). Positively and negatively charged residues are colored red and blue, respectively. Note that the first three residues (PEP) of the H2B tail in *Xenopus laevis* are missing in PDB[69] entry 1KX5[3]. Therefore, the number of the first residue (Ala) in crystal structure 1KX5[3], which we employed, corresponds to the fourth residue in *X. laevis*.

lesion modification site are given in Figure S1. Similarly, we acetylated lysine residues in the tail for the lesion-containing case (*lesion-containing/acetylated* NCP).

Simulation Methods. For the simulations of these four NCP models, we conducted ~3−3.5 μs MD simulations using the AMBER14[71] package with force field *ff*14SB[72] for histones and incorporated modifications[73−75] for nucleosomal DNA. We used the Joung−Cheatham[76] model for the K^+ ions. The TIP3P[77] model was used for water, and K^+ ions were added to neutralize the system. The number of waters, box sizes, and the length of the simulation for the investigated NCP models are summarized in Table S1.

Postprocessing of all simulations was carried out using the CPPTRAJ[78] module of AMBER14.[71] All structural analyses were obtained from these MD simulations with the first 1.5 μs discarded. This was based on the two-dimensional (2D) RMSDs (Figure S2) of the tail conformation, showing that stable tail structures were achieved after ~1.5 μs in the *lesion-free/unacetylated* NCP. In other NCP cases, the structures fluctuated throughout the simulations compared to the structure of this *lesion-free/unacetylated* NCP.

PyMOL (The PyMOL Molecular Graphic System, version 1.3x, Schrödinger, LLC) and VMD[79] were employed for molecular modeling, images, and movies.

Full details concerning preparation of NCP models, the force field, the MD simulation protocol, and structural analyses are given in the Methods section of the Supporting Information.

RESULTS

In the *Lesion-Free/Unacetylated* NCP, the Tail Is Collapsed onto the DNA Surface, Unstructured and Extended. We have investigated the structure and dynamics of the H2B tail in the *lesion-free/unacetylated* NCP, with ~3 μs MD simulation. In the initial model (see Materials and Methods), the H2B tail residues are mostly between the two DNA gyres at SHL ~ 3. The snapshots of the tail along the MD simulation (Figure S3) show that the tail remains between the two gyres initially up to ~1 μs. Afterward, the tail becomes transiently solvent exposed (Figure S3C), and subsequently, at ~1.5 μs, the tail collapses onto one of the DNA gyres [gyre-1 (Figure 2A and Movie S1)], interacts stably with the DNA surface (Figure 2B and Figure S4A), and forms an extended conformation (Figure 2C). Because of the stable collapse of the tail onto the DNA, the tail dynamics is inhibited, as revealed in ensemble average RMSF values in Figure 2A, and the tail samples a limited conformational space (Figure S2A).

In this collapsed and extended state of the tail, there are favorable electrostatic interactions between the negatively charged DNA phosphate groups and the large proportion of positively charged lysine and arginine residues in the tail (14 lysine and arginine residues of 34 tail residues, shown in Figure 1C); electrostatic repulsions between positively charged lysine residues are minimized because of the increased pairwise distances between these charged residues, and DNA−tail electrostatic attractions are optimized with extension of the tail (Figure 2B, Table S2, and Figure S5). The tail extension is quantitatively revealed in the radii of gyration (Figure 2C), which show a narrowly clustered population that is closer to an extended, denatured random coil than to a compact, globular state. Consistent with the extended state of the tail, helical content (Figure 2D), including α-helix and 3_{10}-helix, is very limited. It occurs only between residues 14 and 17 (corresponding to residues Ala14, Val15, Thr16, and Lys17), is only ~33% of the population, and is absent in other regions of the tail.[80] Furthermore, the helices are unstable, fluctuating between helical and turn conformations every few nanoseconds

DOI: 10.1021/acs.biochem.6b01208
Biochemistry 2017, 56, 1963−1973

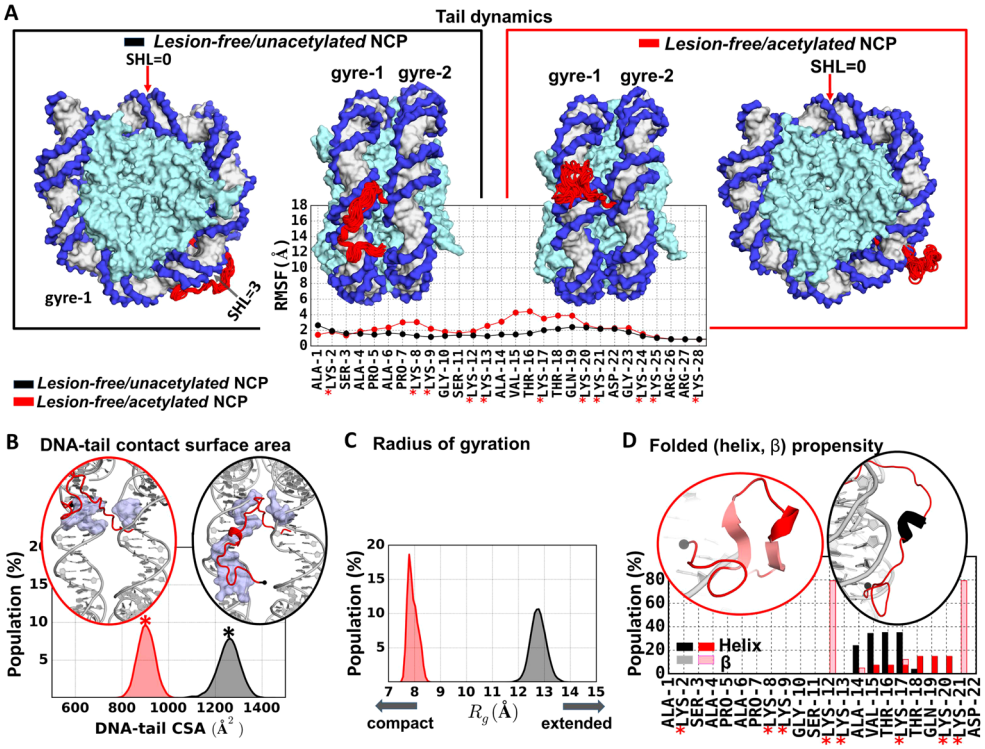

Figure 2. Impact of lysine acetylation on the histone H2B tail in lesion-free NCPs. (A) Acetylation causes the tail to be released from the DNA, which makes it more solvent-exposed and dynamic. This is shown in the greater ensemble average values of the tail backbone heavy atom root-mean-squared fluctuations (RMSF), and in the tail ensemble structures. Top and side views are given. (B) Acetylation reduces the DNA−tail contact surface area (CSA), as shown by the distributions of the DNA−tail CSA. Details of specific interactions between DNA base pairs and histone tail amino acids are given in Figure S4. Structures shown, designated by an asterisk on the CSA, are representative of the highest-population clusters. Acetylation causes the tail to be more compact. This is shown in panel C by the distributions of the tail radii of gyration (R_g) and by (D) their increased folded, helix and β-strand, propensity. In panel A, the best representative NCP structure from the MD ensemble is shown, except for the H2B tail for which snapshots at 100 ns intervals are presented; the H2B N-terminal tail is rendered as a red cartoon, the histone core as a cyan surface, and the DNA as a surface with a blue backbone and gray bases. In panels B and D, the Cα atom of the first residue from the N-terminus is shown as a black dot. See Movies S1 and S2.

(Figure S6A). Favorable electrostatic interactions between lysine residues and the DNA backbone impede formation of stable helical forms in the tail,[81] and repulsions between positively charged lysine residues that are near each other also destabilize compact helical structures.[42,50] Prior MD simulations have also revealed collapse of the histone tails on the nucleosomal DNA,[55,81−85] as well as transient helical states in the tails.[81,84]

In the *Lesion-Free/Acetylated* NCP, the Tail Is Released from the DNA Surface and Assumes a Compact Structure. We wished to explore the effect that lysine acetylation has on the tail structure and dynamics. The overarching impact of lysine acetylation on the histone tail is due to attendant charge neutralization and increased hydrophobicity, and important effects of the acetylation stem from these phenomena. Specifically, N-terminal tail residues 1−25 are released from the DNA surface, especially on the major groove side, and adopt a compact conformation that is modestly more dynamic than the unacetylated tail, as shown in Figure 2A. The release of the tail from the DNA is explained by the significant reduction in the strength of favorable DNA−tail interactions upon acetylation (Figure 2B, Table S3 and Figure S4B, and Movie S2). Nonetheless, the tail remains in the vicinity of the DNA. Furthermore, these weakened DNA−tail interactions cause the DNA to be more dynamic (Figure S7), including greater fluctuations in the minor groove widths (Figure S8).

The compaction of the tail is due to decreased intratail repulsion between the positively charged lysine residues and increased intratail hydrophobic interactions, such as van der Waals interactions between acetyl methyl groups, that shorten the distance between them (Figure S5). The radii of gyration quantitatively demonstrate this compaction, with the peak greatly shifted toward the compact globular domain (Figure 2C). Furthermore, the tail adopts a stable β-hairpin conformation, involving residues 12−21, with flickering helical structure within these residues (Figure 2D and Figure S6B), which is consistent with the tail compaction.

In the *Lesion-Containing/Unacetylated* NCP, Part of the Tail Is Stably Engulfed by the B[*a*]P Rings while Part Is Fully Solvent Exposed. Our prior 800 ns MD study[57] of the NCP containing the DNA minor groove B[a]P-dG lesion (see the inset box in Figure 1), positioned at SHL ∼ 3 near the H2B tail, showed that part of the tail is tightly engulfed by the B[a]P ring system's enlarged minor groove. Here we extended the simulation to ∼3.5 μs. We wished to further assess the stability of the tail entrapment, to consider the characteristics of the unengulfed part of the tail, and to elucidate the impact of lysine acetylation on the entire tail, including its entrapped region and beyond.

DOI: 10.1021/acs.biochem.6b01208
Biochemistry 2017, 56, 1963−1973

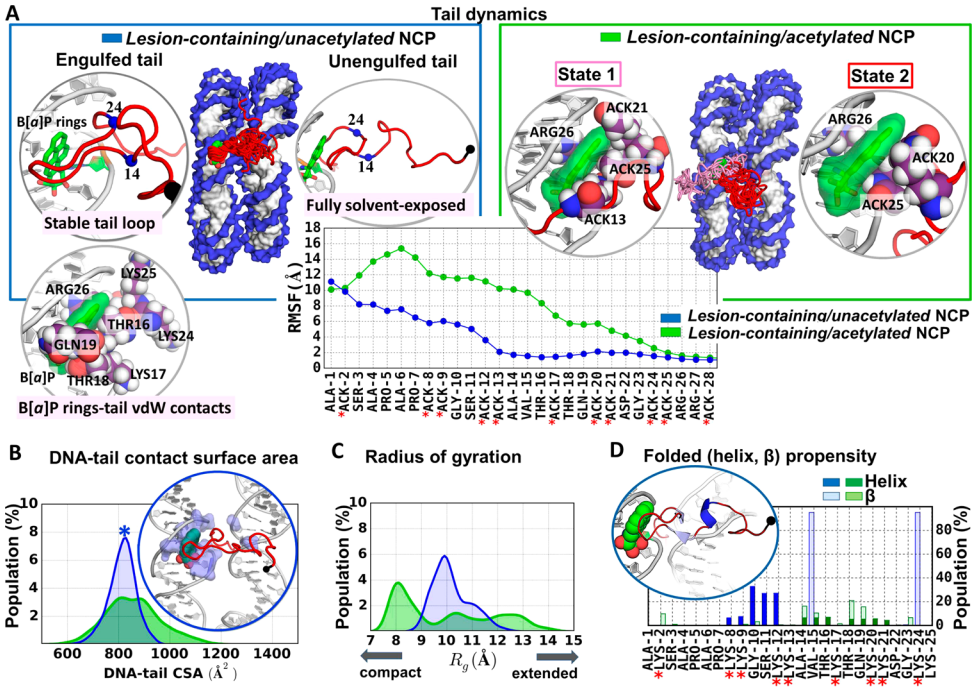

Figure 3. Impact of the minor groove-situated B[*a*]P-dG lesion on the histone H2B tail in lesion-containing NCPs. (A) The state of acetylation of the H2B tail determines the stability of its engulfment by the B[*a*]P ring system. The unacetylated tail residues 14−26 form a stable loop, and most of these residues are tightly entrapped in the lesion-imposed enlarged minor groove (see "Engulfed tail" in the blue box); the first 13 residues from the N-terminus become solvent-exposed (see "Unengulfed tail" in the blue box). The acetylated tail oscillates between two conformations, one (state 1) in which it is in the lesion-containing minor groove and a second (state 2) where it is housed between the two DNA gyres (right panel, green box). The van der Waals interactions between the B[*a*]P ring system and the tail residues (ACK13, ACK20, ACK21, and ACK25) are always unstable (Figure S10), causing the acetylated tail to be dynamic, as shown in the greater ensemble average RMSF values, and in the tail ensemble structures. (B) DNA−tail contact surface areas (CSA) are similar in both unacetylated (mean values of 813 ± 54 Å^2) and acetylated (mean values of 858 ± 110 Å^2) NCPs; however, the CSA is broader and bimodal in the acetylated NCP, while there is a single sharp peak for the unacetylated case and the structure shown, designated by an asterisk on the CSA, is representative of the highest-population cluster. Details of specific interactions between DNA base pairs and histone tail amino acids are given in Figure S4. (C) The distributions of the tail radii of gyration (R_g) also reveal a single peak in the unacetylated tail and bimodal states in the acetylated case, with state 1 extended and state 2 compact, revealing great conformational variability. (D) The lesion inhibits helical conformations by interacting with the tail, as shown by the decreased helical propensity in the engulfed region. In panel A, the best representative NCP structure from the MD ensemble is shown, except for the H2B tail for which snapshots at 100 ns intervals are presented; the H2B N-terminal tail is rendered as a red cartoon, the histone core as a cyan surface, and the DNA as the surface with a blue backbone and gray bases. In panels B and D, the Cα atom of the first residue from the N-terminus is shown as a black dot. See Movies S3 and S4.

Our extended simulation shows that the features of the engulfed tail from the first 800 ns simulation persist to 3.5 μs; tail residues 14−24 form a stable loop, and most residues between positions 16 and 26 are collapsed stably on the B[*a*]P ring system in the enlarged minor groove (Figure 3A, Figure S8A, and Movie S3). Therefore, most DNA−tail contacts are in the lesion-containing minor groove (Figure 3B and Figure S4C). The tail entrapment is stabilized by a network of interactions: favorable van der Waals (Figure S9A), hydrogen bonds (Figure S9B and Table S4), and methyl−π (*Me*−π) interactions (Figure S9C) between the B[*a*]P aromatic rings and the tail, as well as interactions between the DNA and the tail (Table S5). Figure 3A and Figure S9A show specific van der Waals interactions between B[*a*]P rings and amino acids Thr16, Lys17, Thr18, Gln19, and Arg26. In addition, intratail hydrogen bond interactions contribute to the stability of the tail loop (Table S6 and Figure S9D,E), causing the tail in this region to be more compact (Figure 3C), with a stable β-hairpin loop (Figure 3D).

Beyond the engulfed region, tail residues 1−12 are released from the DNA, solvent-exposed, and mobile (Figure 3A and Movie S3). Therefore, the DNA−tail contact surface area is significantly reduced by the presence of the lesion, with a peak value of ∼800 Å^2 (Figure 3B), compared to the peak value of ∼1300 Å^2 for the *lesion-free/unacetylated* NCP (Figure 2B). The enhanced mobility of these released residues is revealed in their ensemble average RMSF values (Figure 3A) and also the wider distribution of their radii of gyration (Figure 3C). The released tail residues are mostly unstructured, adopting ∼30% flickering helical conformations between residues 8 and 12 (Figure 3D and Figure S6C). Because of the released N-terminal tail residues, the DNA near the lesion, including the minor groove widths (Figure S8), is more dynamic compared to the lesion-free case (Figure S7).

In the *Lesion-Containing/Acetylated* NCP, the Tail Undergoes Large Conformational Transitions between Two States while Maintaining Contact with the B[*a*]P Rings. The B[*a*]P ring system remains an attractor to the tail residues in the *lesion-containing/acetylated* NCP. When the lysine residues are acetylated, the tail becomes less charged and more hydrophobic; hence, the DNA−tail interactions are weakened (Table S7 and Figure S4D). However, van der Waals interactions between the B[*a*]P rings and the tail remain, specifically between the acetyl-lysine side chain and the B[*a*]P

DOI: 10.1021/acs.biochem.6b01208
Biochemistry 2017, 56, 1963−1973

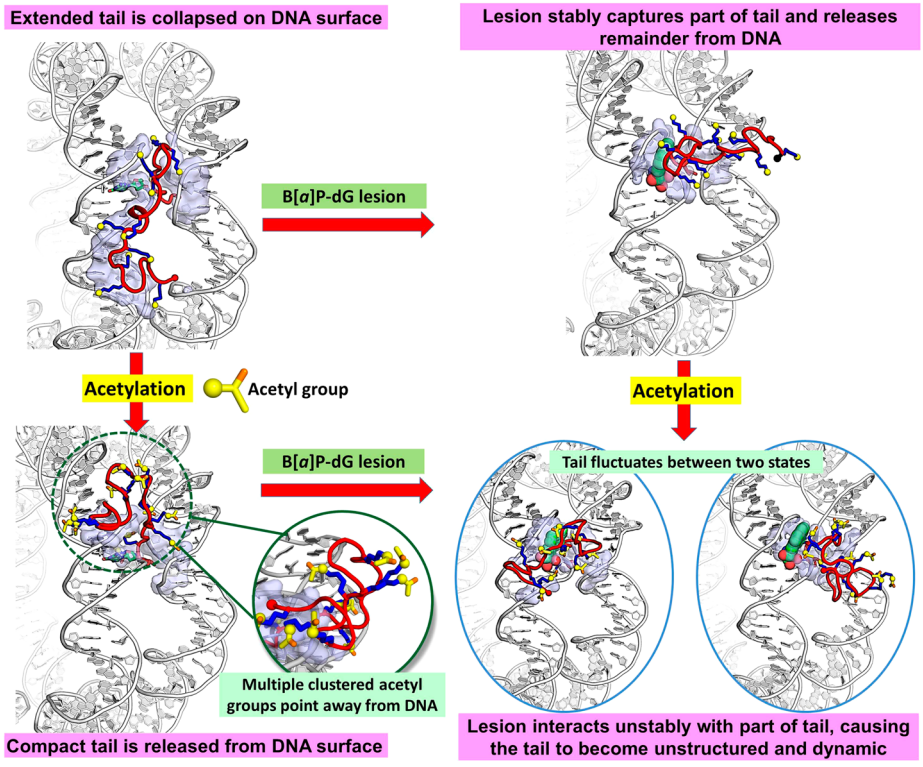

Figure 4. Impact of lysine acetylation and the presence of the lesion on the tail conformation in the NCP, showing that the lesion disrupts the normal tail behavior. Color code: DNA, gray; H2B tail, red; lysine or acetyl-lysine residues, blue sticks; acetyl group, colored by atom with yellow carbons; B[*a*]P ring system, colored by atom with green carbons; DNA–tail contact surface area, light blue surface.

rings, but these interactions fluctuate greatly because of the weakened electrostatic interactions (Figures S10 and S11). Hence, the tail oscillates mainly between two conformations (Figure 3A and Movie S4): in one conformation (state 1), the tail is in the lesion-containing minor groove and has relatively more van der Waals interactions with the lesion rings; in the second conformation (state 2), the tail is housed between the two gyres and has relatively fewer van der Waals interactions with the lesion rings. Regardless of the state, the tail always contacts the B[*a*]P aromatic rings through mainly van der Waals and hydrogen bond (Table S8) interactions, although unstably. Analyses of the two separately clustered states of the tail are given in Figure S12.

Ensemble average values for various tail characteristics are in line with the tail conformational interchange. The tail residues are very dynamic as shown in their RMSF values (Figure 3A). The distribution of the DNA–tail CSA is broad (Figure 3B), and there are multiple populations (state 1, state 2, and intermediate states) in the tail radii of gyration (Figure 3C): the population with the tail between the two gyres has a peak at ∼8 Å that is near the globular domain and is compact because of internal van der Waals interactions within the tail that involve acetyl groups; the second population with tail in the minor groove has larger radii of gyration, reflecting its greater extension. Notably, the folded propensities (helical and β structures) of the acetylated tail are greatly reduced by the presence of the lesion regardless of the states (Figure 3D), because the lesion–tail interactions outcompete the intratail hydrogen bonds needed to form the helical or β conformations. Therefore, the interactions between the histone tail and the B[*a*]P ring system tend to destabilize the tail folded structures.

Lysine acetylation not only causes the tail to be more dynamic but also allows the DNA to be more dynamic (Figure S7), including increased minor groove dynamics (Figure S8B). Among our investigated systems, the DNA is the most dynamic when the lesion is present and the tail is acetylated.

DISCUSSION

In this study, we wished to gain insight into how the presence of a lesion derived from the carcinogen benzo[*a*]pyrene in the nucleosome would likely disrupt the multiple biological functions of histone tails, in both unacetylated and acetylated states. For this purpose, we have performed four simulations of NCP models, namely, *lesion-free/unacetylated*, *lesion-free/acetylated*, *lesion-containing/unacetylated*, and *lesion-containing/acetylated* NCPs. We have utilized ∼3 μs molecular dynamics simulations of individual NCP models to obtain a detailed understanding of the impact that a benzo[*a*]pyrene-derived DNA lesion, B[*a*]P-dG, and lysine acetylation have on the tail structures, dynamics, and interactions with nucleosomal DNA. Our MD simulations focus on only a single H2B tail; this has an advantage in that it permits pinpointing the structures and interactions among a single tail, the local DNA, and the carcinogen. However, it neglects the effects of the other tails on these phenomena, which is a fertile area for exploration, particularly involving DNA lesions. Experimental studies have shown for the histone tails that their functions are not necessarily independent.[32] In addition, we acetylated all lysines in the H2B tail; this optimizes the possibility of defining the structural and dynamic impacts of acetylation and has the advantage of avoiding the need to choose specific lysines for acetylation, because these are variable and species-dependent.[18,55,86] For each case, we have analyzed in detail structural

DOI: 10.1021/acs.biochem.6b01208
Biochemistry 2017, 56, 1963–1973

and dynamic properties of the H2B tail; specifically, we have evaluated DNA−tail interactions, the DNA and tail dynamics, and tail structures and have determined how the lesion inhibits the normal tail behavior in unacetylated and acetylated states. A summary of our key findings is given in Figure 4.

Acetylation Reduces DNA−Tail Contacts, Making DNA and the Tail Available for Other Interactions. Our results showed, in the case of the lesion-free NCPs, that the unacetylated tail is collapsed onto the DNA surface while the acetylated tail, released from the DNA surface but remaining in its vicinity, assumes a more compact structure. These phenomena result from the lysine charge neutralization upon acetylation; electrostatic DNA−histone attractions and histone−histone repulsions are decreased, and hydrophobic interactions among the tail acetyl groups are increased (Figure S5). Therefore, acetylation reduces the level of contact between the DNA and the tail (Figure 2B), thereby allowing the unbound DNA to be more dynamic (Figure S7) and accessible. In addition, the released tail contains persistent β-hairpin structures that contain flickering helices within the loop (Figure 2D), which render the tail more compact (Figure 2C). The well-known function of lysine acetylation in facilitating DNA accessibility[34,45−47] would be promoted by the release of the tail from the DNA, the attendant enhanced DNA mobility, and the compaction of the released tail. Other computational studies have supported the possibility that acetylation causes a decreased level of DNA−tail contact[50,53,55] and increased compaction of the tail due to formation of secondary structure.[49,50,52,53,55,56] Moreover, the helical and β content and the balance between them may depend on the specific tail. In addition, various experiments have revealed that acetylation increases DNA dynamics, nucleosome accessibility, and tail helical structure content. A crystal structure of a NCP with a tetra-acetylated H4 tail and an unacetylated tail showed that acetylation increased the *B*-factor (reflecting mobility) of nearby DNA.[43] It was recently reported that when the histone H4 tail is modified by "acetylation mimics", in which positively charged lysines are replaced by uncharged glutamines, accessibility in the immediate vicinity of the nucleosome is increased. When the H3 tail was additionally modified similarly, there was a synergistic effect to further increase the nucleosome accessibility.[45] Circular dichroism (CD) studies[42] have shown increased α-helical content with acetylation, consistent with a more compact conformation of the investigated H4 tail.

Our simulations may help provide molecular interpretations of the interesting experimental work of Wang and Hayes,[87] who studied the effect of mimics of up to nine lysine acetylations on the interactions of the H2B tail with DNA. Structurally, in our simulations, the tail is extended (elongated) and collapsed onto the DNA surface when unacetylated; however, when acetylated, it is more condensed (Figure 2C) with enhanced folded states (Figure 2D) and released from the DNA, while remaining in its vicinity (Figure 2B). This is consistent with the suggestion[87] that acetylation "causes localized alterations in tail binding. These alterations may be related to specific structural changes in tail structure detected by spectroscopic techniques".[42,88]

It has been suggested that tail compaction decreases the tail availability for crucial internucleosomal interactions in chromatin compaction[53] and induces unwrapping of linker DNA to provide greater access to the DNA.[50] The more condensed tail conformation could act as a docking site for acetyl-lysine binding proteins; this is in line with a structural study that highlights the importance of multiply acetylated tails, which has shown that closely packed, clustered acetylation sites provide recognition motifs for hydrophobic cavities in acetyl-lysine binding proteins.[14]

Engulfment of Part of the Tail by the B[*a*]P-dG Lesion Would Disrupt Critical Tail Functions. In the presence of the B[*a*]P-dG lesion, a part of the unacetylated tail is stably engulfed by the B[*a*]P ring system. When the tail is acetylated, it still partly contacts the B[*a*]P rings, mainly through van der Waals interactions via acetyl groups, but the interactions are unstable (Figures S10 and S11); the tail oscillates between being housed in the lesion-containing minor groove or between the two gyres (Figure 3A), due to competing interactions between the tail and B[*a*]P rings or intratail interactions. Consequently, in the tail−DNA contact pattern, the DNA and the tail are more dynamic in the acetylated case (Figure 3).

The B[*a*]P-dG lesion's partial entrapment of the tail should hinder the tail from interacting with other nucleosomes, and other proteins such as acetylases, deacetylases, and acetyl-lysine binding proteins, and thereby disrupt critical tail functions. Thus, the entrapped tail would inhibit acetylation/deacetylation or other modifications for achieving access to the DNA. Furthermore, engulfment of part of the tail limits the ability of the tail to extend or compact when needed. This limitation to extension for the unacetylated tail would inhibit the ability of the tail to reach out to neighboring nucleosomes and thereby weaken crucial histone−histone or histone−DNA interactions and possibly lead to chromatin decondensation; the restraint on compaction for the acetylated tail could prevent formation of structural motifs needed for recognition by various chromatin remodeling proteins.[14]

Recently, it has been found that acrolein, a major component of cigarette smoke and cooking fumes, reacts with histone H4 tail lysine residues to form an acrolein adduct, which inhibits lysine acetylation and therefore disrupts interactions of the tail with binding factors needed for nucleosome[41] and chromatin assembly.[89,90] Greenberg and co-workers have shown that DNA abasic lesions react with tail lysine residues to form cross-links whose rates of formation depend on the translational setting of the lesion in the nucleosome; furthermore, they have suggested that such cross-links would impede histone tail post-translational modifications.[91,92] Additionally, it has recently been shown for histone H2B *in vivo*, that the suspected human carcinogen furan can produce a cross-link adduct with a nontail lysine residue that is crucial for nucleosome stability and a target for PTMs; impaired PTM and subsequent alterations in gene expression could result.[93] Finally, our findings that the DNA is more dynamic with the B[*a*]P-dG lesion present, and even more so when the tail is acetylated, suggest that this mobility may be a signal that facilitates access to the lesion by the nucleotide excision repair machinery, which is responsible for their removal, according to the "access, repair, restore" paradigm pioneered by Smerdon.[94,95]

In conclusion, our molecular dynamics simulations suggest that interactions of histone tails with bulky DNA lesions would impede the normal functions of the tails that are currently of great interest but yet poorly understood. The roles of the different tails and how these interact with different lesions, which may be positioned at various rotational and translational settings, are areas of great interest for future work.

DOI: 10.1021/acs.biochem.6b01208
Biochemistry 2017, 56, 1963−1973

■ ASSOCIATED CONTENT

Supporting Information

The Supporting Information is available free of charge on the ACS Publications website at DOI: 10.1021/acs.biochem.6b01208.

Supplementary methods, details of the MD simulations for the investigated NCP models (Table S1), hydrogen bond analyses between DNA and the tail in the *lesion-free/unacetylated* NCP (Table S2), hydrogen bond analyses between DNA and the tail in the *lesion-free/acetylated* NCP (Table S3), hydrogen bond analyses between tail lysine 17 and the B[*a*]P ring system in the *lesion-containing/unacetylated* NCP (Table S4), hydrogen bond analyses between DNA and the tail in the *lesion-containing/unacetylated* NCP (Table S5), hydrogen bond analyses between the residues within the tail in the *lesion-containing/unacetylated* NCP (Table S6), hydrogen bond analyses between DNA and the tail in the *lesion-containing/acetylated* NCP (Table S7), hydrogen bond analyses between tail acetylated lysine residues and the B[*a*]P ring system in the *lesion-containing/acetylated* NCP (Table S8), structure and sequence of DNA gyres around the H2B tail (Figure S1), 2D RMSDs of four investigated NCPs (Figure S2), tail trajectory along the MD simulation in the *lesion-free/unacetylated* NCP (Figure S3), contact maps between DNA and tail residues in the NCPs (Figure S4), DNA−lysine/acetylated lysine residue contact surface area and pairwise distances of lysine/acetylated lysine residues in the tail in lesion-free NCPs (Figure S5), secondary structure of the tail in the NCPs (Figure S6), RMSFs of the DNA in the NCPs (Figure S7), minor groove width in the NCPs (Figure S8), entrapment of the tail by the B[*a*]P ring system through a network of interactions in the *lesion-containing/unacetylated* NCP (Figure S9), van der Waals interaction energies between the B[*a*]P ring system and tail residues in the *lesion-containing/acetylated* NCP (Figure S10), comparison of the tail−lesion aromatic ring van der Waals interactions (Figure S11), and structural and dynamics analyses of two conformations of the tail in the *lesion-containing/acetylated* NCP (Figure S12) (PDF)

Best representative structure of the *lesion-free/unacetylated* NCP (Movie S1) (AVI)

Best representative structure of the *lesion-free/acetylated* NCP (Movie S2) (AVI)

Entrapment of the tail by the B[*a*]P-dG lesion in the *lesion-containing/unacetylated* NCP (Movie S3) (AVI)

Entrapment of the tail by the B[*a*]P-dG lesion in the *lesion-containing/acetylated* NCP (Movie S4) (AVI)

■ AUTHOR INFORMATION

Corresponding Author

*E-mail: broyde@nyu.edu. Telephone: (212) 998-8231. Fax: (212) 995-4015.

ORCID

Suse Broyde: 0000-0002-3802-7511

Funding

This work was supported by NIH, NIEHS Grant R01-ES025987 and NCI Grants R01-CA28038 and R01-CA75449 (to S.B.) and R01-CA168469 (to N.E.G.), and NIGMS Grant R01-GM079223 (to Y.Z.).

Notes

The authors declare no competing financial interest.

■ ACKNOWLEDGMENTS

We gratefully acknowledge resources provided by the Extreme Science and Engineering Discovery Environment (XSEDE), which is supported by National Science Foundation (NSF) Grant MCB060037 to S.B., and the NYU IT High Performance Computing Resources and Services.

■ ABBREVIATIONS

B[*a*]P, benzo[*a*]pyrene; B[*a*]P-dG, 10*S* (+)-*trans-anti*-B[*a*]P-N^2-dG; CD, circular dichroism; CSA, contact surface area(s); MD, molecular dynamics; NER, nucleotide excision repair; NCP, nucleosome core particle; PAH, polycyclic aromatic hydrocarbon; PDB, Protein Data Bank; PTM, post-translational modification; RMSD, root-mean-square deviation; RMSF, root-mean-square fluctuation; SHL, superhelical location; UV, ultraviolet.

■ REFERENCES

(1) McGhee, J. D., and Felsenfeld, G. (1980) Nucleosome structure. *Annu. Rev. Biochem. 49*, 1115−1156.

(2) Luger, K., Mader, A. W., Richmond, R. K., Sargent, D. F., and Richmond, T. J. (1997) Crystal structure of the nucleosome core particle at 2.8 Å resolution. *Nature 389*, 251−260.

(3) Davey, C. A., Sargent, D. F., Luger, K., Maeder, A. W., and Richmond, T. J. (2002) Solvent mediated interactions in the structure of the nucleosome core particle at 1.9 Å resolution. *J. Mol. Biol. 319*, 1097−1113.

(4) Luger, K., and Richmond, T. J. (1998) The histone tails of the nucleosome. *Curr. Opin. Genet. Dev. 8*, 140−146.

(5) Kouzarides, T. (2007) Chromatin modifications and their function. *Cell 128*, 693−705.

(6) Bannister, A. J., and Kouzarides, T. (2011) Regulation of chromatin by histone modifications. *Cell Res. 21*, 381−395.

(7) Mao, P., and Wyrick, J. J. (2016) Emerging roles for histone modifications in DNA excision repair. *FEMS Yeast Res. 16*, fow090.

(8) Mutskov, V., Gerber, D., Angelov, D., Ausio, J., Workman, J., and Dimitrov, S. (1998) Persistent interactions of core histone tails with nucleosomal DNA following acetylation and transcription factor binding. *Mol. Cell. Biol. 18*, 6293−6304.

(9) Angelov, D., Vitolo, J. M., Mutskov, V., Dimitrov, S., and Hayes, J. J. (2001) Preferential interaction of the core histone tail domains with linker DNA. *Proc. Natl. Acad. Sci. U. S. A. 98*, 6599−6604.

(10) Dorigo, B., Schalch, T., Bystricky, K., and Richmond, T. J. (2003) Chromatin fiber folding: requirement for the histone H4 N-terminal tail. *J. Mol. Biol. 327*, 85−96.

(11) Marmorstein, R., and Trievel, R. C. (2009) Histone modifying enzymes: structures, mechanisms, and specificities. *Biochim. Biophys. Acta, Gene Regul. Mech. 1789*, 58−68.

(12) Taverna, S. D., Li, H., Ruthenburg, A. J., Allis, C. D., and Patel, D. J. (2007) How chromatin-binding modules interpret histone modifications: lessons from professional pocket pickers. *Nat. Struct. Mol. Biol. 14*, 1025−1040.

(13) Filippakopoulos, P., and Knapp, S. (2014) Targeting bromodomains: epigenetic readers of lysine acetylation. *Nat. Rev. Drug Discovery 13*, 337−356.

(14) Filippakopoulos, P., Picaud, S., Mangos, M., Keates, T., Lambert, J. P., Barsyte-Lovejoy, D., Felletar, I., Volkmer, R., Muller, S., Pawson, T., Gingras, A. C., Arrowsmith, C. H., and Knapp, S. (2012) Histone recognition and large-scale structural analysis of the human bromodomain family. *Cell 149*, 214−231.

(15) Musselman, C. A., Lalonde, M. E., Cote, J., and Kutateladze, T. G. (2012) Perceiving the epigenetic landscape through histone readers. *Nat. Struct. Mol. Biol. 19*, 1218−1227.

DOI: 10.1021/acs.biochem.6b01208
Biochemistry 2017, 56, 1963−1973

(16) Musselman, C. A., Gibson, M. D., Hartwick, E. W., North, J. A., Gatchalian, J., Poirier, M. G., and Kutateladze, T. G. (2013) Binding of PHF1 Tudor to H3K36me3 enhances nucleosome accessibility. *Nat. Commun. 4*, 2969.
(17) Kurdistani, S. K., and Grunstein, M. (2003) Histone acetylation and deacetylation in yeast. *Nat. Rev. Mol. Cell Biol. 4*, 276−284.
(18) Koprinarova, M., Schnekenburger, M., and Diederich, M. (2016) Role of histone acetylation in cell cycle regulation. *Curr. Top. Med. Chem. 16*, 732−744.
(19) Verdone, L., Agricola, E., Caserta, M., and Di Mauro, E. (2006) Histone acetylation in gene regulation. *Briefings Funct. Genomics Proteomics 5*, 209−221.
(20) Grunstein, M. (1997) Histone acetylation in chromatin structure and transcription. *Nature 389*, 349−352.
(21) Xu, Y., and Price, B. D. (2011) Chromatin dynamics and the repair of DNA double strand breaks. *Cell Cycle 10*, 261−267.
(22) Bird, A. W., Yu, D. Y., Pray-Grant, M. G., Qiu, Q., Harmon, K. E., Megee, P. C., Grant, P. A., Smith, M. M., and Christman, M. F. (2002) Acetylation of histone H4 by Esa1 is required for DNA double-strand break repair. *Nature 419*, 411−415.
(23) Nag, R., Kyriss, M., Smerdon, J. W., Wyrick, J. J., and Smerdon, M. J. (2010) A cassette of N-terminal amino acids of histone H2B are required for efficient cell survival, DNA repair and Swi/Snf binding in UV irradiated yeast. *Nucleic Acids Res. 38*, 1450−1460.
(24) Yu, S., Teng, Y., Waters, R., and Reed, S. H. (2011) How chromatin is remodelled during DNA repair of UV-induced DNA damage in Saccharomyces cerevisiae. *PLoS Genet. 7*, e1002124.
(25) Duan, M. R., and Smerdon, M. J. (2014) Histone H3 lysine 14 (H3K14) acetylation facilitates DNA repair in a positioned nucleosome by stabilizing the binding of the chromatin Remodeler RSC (Remodels Structure of Chromatin). *J. Biol. Chem. 289*, 8353−8363.
(26) Ramanathan, B., and Smerdon, M. J. (1989) Enhanced DNA repair synthesis in hyperacetylated nucleosomes. *J. Biol. Chem. 264*, 11026−11034.
(27) Waters, R., van Eijk, P., and Reed, S. (2015) Histone modification and chromatin remodeling during NER. *DNA Repair 36*, 105−113.
(28) Glozak, M. A., and Seto, E. (2007) Histone deacetylases and cancer. *Oncogene 26*, 5420−5432.
(29) Kuo, C. H., Hsieh, C. C., Lee, M. S., Chang, K. T., Kuo, H. F., and Hung, C. H. (2014) Epigenetic regulation in allergic diseases and related studies. *Asia Pacific Allergy 4*, 14−18.
(30) Lee, J., Hwang, Y. J., Kim, K. Y., Kowall, N. W., and Ryu, H. (2013) Epigenetic mechanisms of neurodegeneration in Huntington's disease. *Neurotherapeutics 10*, 664−676.
(31) Peleg, S., Feller, C., Ladurner, A. G., and Imhof, A. (2016) The metabolic impact on histone acetylation and transcription in ageing. *Trends Biochem. Sci. 41*, 700−711.
(32) Gansen, A., Toth, K., Schwarz, N., and Langowski, J. (2015) Opposing roles of H3- and H4-acetylation in the regulation of nucleosome structure–a FRET study. *Nucleic Acids Res. 43*, 1433−1443.
(33) Iwasaki, W., Miya, Y., Horikoshi, N., Osakabe, A., Taguchi, H., Tachiwana, H., Shibata, T., Kagawa, W., and Kurumizaka, H. (2013) Contribution of histone N-terminal tails to the structure and stability of nucleosomes. *FEBS Open Bio 3*, 363−369.
(34) Brower-Toland, B., Wacker, D. A., Fulbright, R. M., Lis, J. T., Kraus, W. L., and Wang, M. D. (2005) Specific contributions of histone tails and their acetylation to the mechanical stability of nucleosomes. *J. Mol. Biol. 346*, 135−146.
(35) Shogren-Knaak, M., Ishii, H., Sun, J. M., Pazin, M. J., Davie, J. R., and Peterson, C. L. (2006) Histone H4-K16 acetylation controls chromatin structure and protein interactions. *Science 311*, 844−847.
(36) Allahverdi, A., Yang, R., Korolev, N., Fan, Y., Davey, C. A., Liu, C. F., and Nordenskiold, L. (2011) The effects of histone H4 tail acetylations on cation-induced chromatin folding and self-association. *Nucleic Acids Res. 39*, 1680−1691.
(37) Robinson, P. J., An, W., Routh, A., Martino, F., Chapman, L., Roeder, R. G., and Rhodes, D. (2008) 30 nm chromatin fibre decompaction requires both H4-K16 acetylation and linker histone eviction. *J. Mol. Biol. 381*, 816−825.
(38) Parra, M. A., Kerr, D., Fahy, D., Pouchnik, D. J., and Wyrick, J. J. (2006) Deciphering the roles of the histone H2B N-terminal domain in genome-wide transcription. *Mol. Cell. Biol. 26*, 3842−3852.
(39) Zheng, S., Crickard, J. B., Srikanth, A., and Reese, J. C. (2014) A highly conserved region within H2B is important for FACT to act on nucleosomes. *Mol. Cell. Biol. 34*, 303−314.
(40) Choi, J., Kim, H., Kim, K., Lee, B., Lu, W., and An, W. (2011) Selective requirement of H2B N-Terminal tail for p14ARF-induced chromatin silencing. *Nucleic Acids Res. 39*, 9167−9180.
(41) Mao, P., Kyriss, M. N., Hodges, A. J., Duan, M., Morris, R. T., Lavine, M. D., Topping, T. B., Gloss, L. M., and Wyrick, J. J. (2016) A basic domain in the histone H2B N-terminal tail is important for nucleosome assembly by FACT. *Nucleic Acids Res. 44*, 9142−9152.
(42) Wang, X., Moore, S. C., Laszckzak, M., and Ausio, J. (2000) Acetylation increases the alpha-helical content of the histone tails of the nucleosome. *J. Biol. Chem. 275*, 35013−35020.
(43) Wakamori, M., Fujii, Y., Suka, N., Shirouzu, M., Sakamoto, K., Umehara, T., and Yokoyama, S. (2015) Intra- and inter-nucleosomal interactions of the histone H4 tail revealed with a human nucleosome core particle with genetically-incorporated H4 tetra-acetylation. *Sci. Rep. 5*, 17204.
(44) Baneres, J. L., Martin, A., and Parello, J. (1997) The N tails of histones H3 and H4 adopt a highly structured conformation in the nucleosome. *J. Mol. Biol. 273*, 503−508.
(45) Mishra, L. N., Pepenella, S., Rogge, R., Hansen, J. C., and Hayes, J. J. (2016) Acetylation mimics within a single nucleosome alter local DNA accessibility in compacted nucleosome arrays. *Sci. Rep. 6*, 34808.
(46) Anderson, J. D., Lowary, P. T., and Widom, J. (2001) Effects of histone acetylation on the equilibrium accessibility of nucleosomal DNA target sites. *J. Mol. Biol. 307*, 977−985.
(47) Polach, K. J., Lowary, P. T., and Widom, J. (2000) Effects of core histone tail domains on the equilibrium constants for dynamic DNA site accessibility in nucleosomes. *J. Mol. Biol. 298*, 211−223.
(48) Yang, D., and Arya, G. (2011) Structure and binding of the H4 histone tail and the effects of lysine 16 acetylation. *Phys. Chem. Chem. Phys. 13*, 2911−2921.
(49) Winogradoff, D., Echeverria, I., Potoyan, D. A., and Papoian, G. A. (2015) The acetylation landscape of the H4 histone tail: disentangling the interplay between the specific and cumulative effects. *J. Am. Chem. Soc. 137*, 6245−6253.
(50) Ikebe, J., Sakuraba, S., and Kono, H. (2016) H3 histone tail conformation within the nucleosome and the impact of K14 acetylation studied using enhanced sampling simulation. *PLoS Comput. Biol. 12*, e1004788.
(51) Saurabh, S., Glaser, M. A., Lansac, Y., and Maiti, P. K. (2016) Atomistic simulation of stacked nucleosome core particles: tail bridging, the H4 tail, and effect of hydrophobic forces. *J. Phys. Chem. B 120*, 3048−3060.
(52) Potoyan, D. A., and Papoian, G. A. (2012) Regulation of the H4 tail binding and folding landscapes via Lys-16 acetylation. *Proc. Natl. Acad. Sci. U. S. A. 109*, 17857−17862.
(53) Collepardo-Guevara, R., Portella, G., Vendruscolo, M., Frenkel, D., Schlick, T., and Orozco, M. (2015) Chromatin unfolding by epigenetic modifications explained by dramatic impairment of internucleosome interactions: a multiscale computational study. *J. Am. Chem. Soc. 137*, 10205−10215.
(54) Chang, L., and Takada, S. (2016) Histone acetylation dependent energy landscapes in tri-nucleosome revealed by residue-resolved molecular simulations. *Sci. Rep. 6*, 34441.
(55) Perisic, O., and Schlick, T. (2016) Computational strategies to address chromatin structure problems. *Phys. Biol. 13*, 035006.
(56) Korolev, N., Yu, H., Lyubartsev, A. P., and Nordenskiold, L. (2014) Molecular dynamics simulations demonstrate the regulation of DNA-DNA attraction by H4 histone tail acetylations and mutations. *Biopolymers 101*, 1051−1064.

DOI: 10.1021/acs.biochem.6b01208
Biochemistry 2017, 56, 1963−1973

(57) Fu, I., Cai, Y., Zhang, Y., Geacintov, N. E., and Broyde, S. (2016) Entrapment of a histone tail by a DNA lesion in a nucleosome suggests the lesion impacts epigenetic marking: a molecular dynamics study. *Biochemistry 55*, 239−242.
(58) International Agency for Research on Cancer (2010) Some non-heterocyclic polycyclic aromatic hydrocarbons and some related exposures. In *IARC Monographs on the Evaluation of Carcinogenic Risks to Humans*, pp 1−853, International Agency for Research on Cancer, Lyon, France.
(59) Conney, A. H. (1982) Induction of microsomal enzymes by foreign chemicals and carcinogenesis by polycyclic aromatic hydrocarbons: G. H. A. Clowes Memorial Lecture. *Cancer Res. 42*, 4875−4917.
(60) Wood, A. W., Chang, R. L., Levin, W., Yagi, H., Thakker, D. R., Jerina, D. M., and Conney, A. H. (1977) Differences in mutagenicity of the optical enantiomers of the diastereomeric benzo[*a*]pyrene 7,8-diol-9,10-epoxides. *Biochem. Biophys. Res. Commun. 77*, 1389−1396.
(61) Brookes, P., and Osborne, M. R. (1982) Mutation in mammalian cells by stereoisomers of anti-benzo[*a*] pyrene-diolepoxide in relation to the extent and nature of the DNA reaction products. *Carcinogenesis 3*, 1223−1226.
(62) Slaga, T. J., Bracken, W. J., Gleason, G., Levin, W., Yagi, H., Jerina, D. M., and Conney, A. H. (1979) Marked differences in the skin tumor-initiating activities of the optical enantiomers of the diastereomeric benzo[*a*]pyrene 7,8-diol-9,10-epoxides. *Cancer Res. 39*, 67−71.
(63) Buening, M. K., Wislocki, P. G., Levin, W., Yagi, H., Thakker, D. R., Akagi, H., Koreeda, M., Jerina, D. M., and Conney, A. H. (1978) Tumorigenicity of the optical enantiomers of the diastereomeric benzo[*a*]pyrene 7,8-diol-9,10-epoxides in newborn mice: exceptional activity of (+)-7beta,8alpha-dihydroxy-9alpha,10alpha-epoxy-7,8,9,10-tetrahydrobenzo[*a*]pyrene. *Proc. Natl. Acad. Sci. U. S. A. 75*, 5358−5361.
(64) Szeliga, J., and Dipple, A. (1998) DNA adduct formation by polycyclic aromatic hydrocarbon dihydrodiol epoxides. *Chem. Res. Toxicol. 11*, 1−11.
(65) Cheng, S. C., Hilton, B. D., Roman, J. M., and Dipple, A. (1989) DNA adducts from carcinogenic and noncarcinogenic enantiomers of benzo[*a*]pyrene dihydrodiol epoxide. *Chem. Res. Toxicol. 2*, 334−340.
(66) Moriya, M., Spiegel, S., Fernandes, A., Amin, S., Liu, T., Geacintov, N., and Grollman, A. P. (1996) Fidelity of translesional synthesis past benzo[*a*]pyrene diol epoxide-2'-deoxyguanosine DNA adducts: marked effects of host cell, sequence context, and chirality. *Biochemistry 35*, 16646−16651.
(67) Cosman, M., de los Santos, C., Fiala, R., Hingerty, B. E., Singh, S. B., Ibanez, V., Margulis, L. A., Live, D., Geacintov, N. E., Broyde, S., and Patel, D. J. (1992) Solution conformation of the major adduct between the carcinogen (+)-*anti*-benzo[*a*]pyrene diol epoxide and DNA. *Proc. Natl. Acad. Sci. U. S. A. 89*, 1914−1918.
(68) Thrall, B. D., Mann, D. B., Smerdon, M. J., and Springer, D. L. (1994) Nucleosome Structure Modulates Benzo[a]Pyrenediol Epoxide Adduct Formation. *Biochemistry 33*, 2210−2216.
(69) Berman, H. M., Westbrook, J., Feng, Z., Gilliland, G., Bhat, T. N., Weissig, H., Shindyalov, I. N., and Bourne, P. E. (2000) The Protein Data Bank. *Nucleic Acids Res. 28*, 235−242.
(70) Ong, M. S., Richmond, T. J., and Davey, C. A. (2007) DNA stretching and extreme kinking in the nucleosome core. *J. Mol. Biol. 368*, 1067−1074.
(71) Case, D. A., Darden, T. A., Cheatham, T. E., III, Simmerling, C. L., Wang, J., Duke, R. E., Luo, R., Walker, R. C., Zhang, W., Merz, K. M., Roberts, B., Wang, B., Hayik, S., Roitberg, A., Seabra, G., Kolossváry, I., Wong, K. F., Paesani, F., Vanicek, J., Liu, J., Wu, X., Brozell, S. R., Steinbrecher, T., Gohlke, H., Cai, Q., Ye, X., Wang, J., Hsieh, M. J., Cui, G., Roe, D. R., Mathews, D. H., Seetin, M. G., Sagui, C., Babin, V., Gusarov, S., Kovalenko, A., and Kollman, P. A. (2014) *AMBER 14*, University of California, San Francisco.
(72) Maier, J. A., Martinez, C., Kasavajhala, K., Wickstrom, L., Hauser, K. E., and Simmerling, C. (2015) ff14SB: Improving the cccuracy of protein side chain and backbone parameters from ff99SB. *J. Chem. Theory Comput. 11*, 3696−3713.
(73) Perez, A., Marchan, I., Svozil, D., Sponer, J., Cheatham, T. E., 3rd, Laughton, C. A., and Orozco, M. (2007) Refinement of the AMBER force field for nucleic acids: improving the description of alpha/gamma conformers. *Biophys. J. 92*, 3817−3829.
(74) Zgarbova, M., Luque, F. J., Sponer, J., Cheatham, T. E., 3rd, Otyepka, M., and Jurecka, P. (2013) Toward Improved Description of DNA Backbone: Revisiting Epsilon and Zeta Torsion Force Field Parameters. *J. Chem. Theory Comput. 9*, 2339−2354.
(75) Cheatham, T. E., 3rd, and Case, D. A. (2013) Twenty-five years of nucleic acid simulations. *Biopolymers 99*, 969−977.
(76) Joung, I. S., and Cheatham, T. E., 3rd (2008) Determination of alkali and halide monovalent ion parameters for use in explicitly solvated biomolecular simulations. *J. Phys. Chem. B 112*, 9020−9041.
(77) Jorgensen, W. L., Chandrasekhar, J., Madura, J. D., Impey, R. W., and Klein, M. L. (1983) Comparison of simple potential functions for simulating liquid water. *J. Chem. Phys. 79*, 926−935.
(78) Roe, D. R., and Cheatham, T. E. (2013) PTRAJ and CPPTRAJ: Software for processing and analysis of molecular dynamics trajectory Data. *J. Chem. Theory Comput. 9*, 3084−3095.
(79) Humphrey, W., Dalke, A., and Schulten, K. (1996) VMD: Visual molecular dynamics. *J. Mol. Graphics 14*, 33−38.
(80) Pace, C. N., and Scholtz, J. M. (1998) A helix propensity scale based on experimental studies of peptides and proteins. *Biophys. J. 75*, 422−427.
(81) Erler, J., Zhang, R., Petridis, L., Cheng, X., Smith, J. C., and Langowski, J. (2014) The role of histone tails in the nucleosome: a computational study. *Biophys. J. 107*, 2911−2922.
(82) Shaytan, A. K., Armeev, G. A., Goncearenco, A., Zhurkin, V. B., Landsman, D., and Panchenko, A. R. (2016) Coupling between histone conformations and DNA geometry in nucleosomes on a microsecond timescale: atomistic insights into nucleosome functions. *J. Mol. Biol. 428*, 221−237.
(83) Anandakrishnan, R., Drozdetski, A., Walker, R. C., and Onufriev, A. V. (2015) Speed of conformational change: comparing explicit and implicit solvent molecular dynamics simulations. *Biophys. J. 108*, 1153−1164.
(84) Sharma, S., Ding, F., and Dokholyan, N. V. (2007) Multiscale modeling of nucleosome dynamics. *Biophys. J. 92*, 1457−1470.
(85) Roccatano, D., Barthel, A., and Zacharias, M. (2007) Structural flexibility of the nucleosome core particle at atomic resolution studied by molecular dynamics simulation. *Biopolymers 85*, 407−421.
(86) Csordas, A. (1990) On the Biological Role of Histone Acetylation. *Biochem. J. 265*, 23−38.
(87) Wang, X., and Hayes, J. J. (2007) Site-specific binding affinities within the H2B tail domain indicate specific effects of lysine acetylation. *J. Biol. Chem. 282*, 32867−32876.
(88) Wang, X., and Hayes, J. J. (2006) Physical methods used to study core histone tail structures and interactions in solution. *Biochem. Cell Biol. 84*, 578−588.
(89) Chen, D., Fang, L., Li, H., Tang, M. S., and Jin, C. (2013) Cigarette smoke component acrolein modulates chromatin assembly by inhibiting histone acetylation. *J. Biol. Chem. 288*, 21678−21687.
(90) Fang, L., Chen, D., Yu, C., Li, H., Brocato, J., Huang, L., and Jin, C. (2016) Mechanisms underlying acrolein-mediated inhibition of chromatin Assembly. *Mol. Cell. Biol. 36*, 2995−3008.
(91) Sczepanski, J. T., Wong, R. S., McKnight, J. N., Bowman, G. D., and Greenberg, M. M. (2010) Rapid DNA-protein cross-linking and strand scission by an abasic site in a nucleosome core particle. *Proc. Natl. Acad. Sci. U. S. A. 107*, 22475−22480.
(92) Weng, L., and Greenberg, M. M. (2015) Rapid histone-catalyzed DNA lesion excision and accompanying protein modification in nucleosomes and nucleosome core particles. *J. Am. Chem. Soc. 137*, 11022−11031.
(93) Nunes, J., Martins, I. L., Charneira, C., Pogribny, I. P., de Conti, A., Beland, F. A., Marques, M. M., Jacob, C. C., and Antunes, A. M. (2016) New insights into the molecular mechanisms of chemical carcinogenesis: In vivo adduction of histone H2B by a reactive

DOI: 10.1021/acs.biochem.6b01208
Biochemistry 2017, 56, 1963−1973

metabolite of the chemical carcinogen furan. *Toxicol. Lett. 264*, 106−113.
(94) Polo, S. E., and Almouzni, G. (2015) Chromatin dynamics after DNA damage: The legacy of the access-repair-restore model. *DNA Repair 36*, 114−121.
(95) Smerdon, M. J., and Lieberman, M. W. (1978) Nucleosome rearrangement in human chromatin during UV-induced DNA-repair synthesis. *Proc. Natl. Acad. Sci. U. S. A. 75*, 4238−4241.

DOI: 10.1021/acs.biochem.6b01208
Biochemistry 2017, 56, 1963−1973